Kinetic Instabilities and Turbulence in the Solar Wind

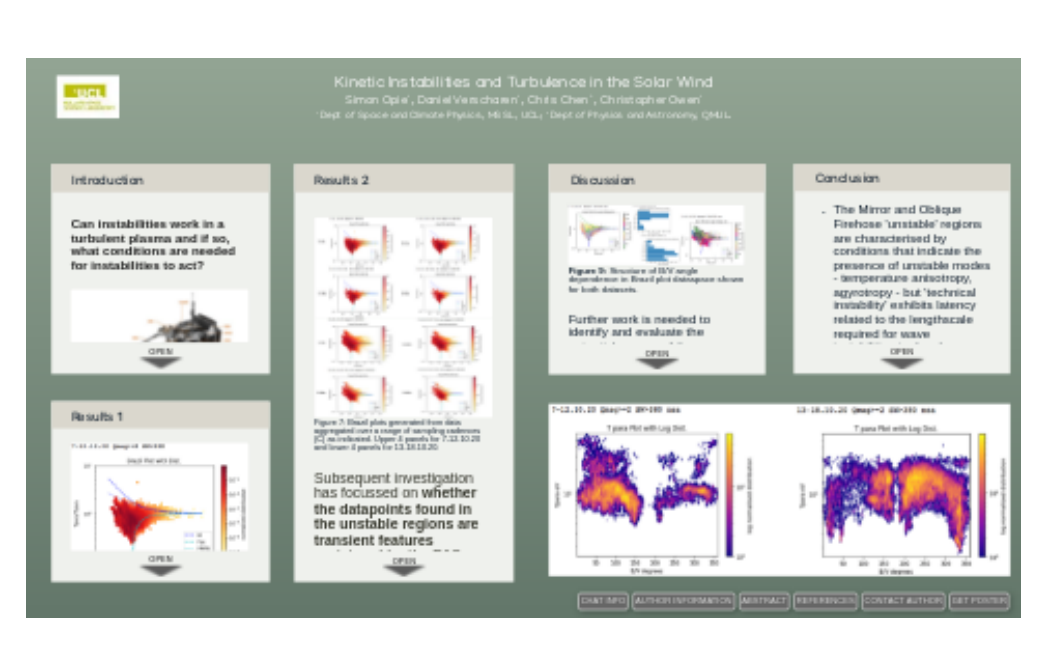

Simon Opie[1] , Daniel Verscharen[1] , Chris Chen[2] , Christopher Owen[1]

[1] Dept of Space and Climate Physics, MSSL, UCL; [2] Dept of Physics and Astronomy, QMUL.

PRESENTED AT:

AGU FALL MEETING
New Orleans, LA & Online Everywhere
13–17 December 2021

Poster Gallery brought to you by WILEY

INTRODUCTION

Can instabilities work in a turbulent plasma and if so, what conditions are needed for instabilities to act?

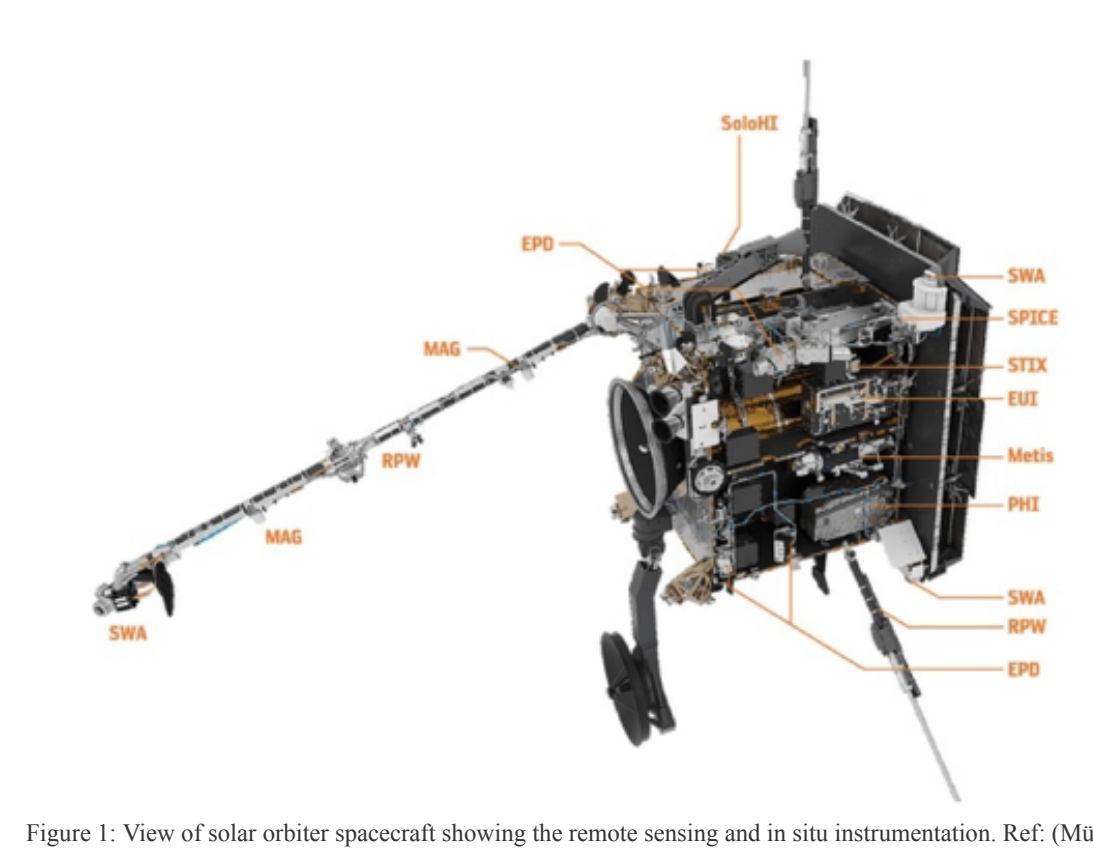

Figure 1: View of solar orbiter spacecraft showing the remote sensing and in situ instrumentation. Ref: (Müller et al., 2020)

This work utilises early data from the Solar Orbiter mission cruise phase. The spacecraft carries 6 remote sensing instruments to observe the Sun's surface and the solar corona and 4 in situ instruments to measure the solar wind, energetic particles and electromagnetic fields.

The various instruments are shown in Figure 1 and for the purposes of this project the instruments of interest are: the Solar Wind Analyser (SWA) for data concerning protons/alpha particles (SWA/PAS) and electrons (SWA/EAS) (Owen et al., 2020); the magnetometer (MAG) for in situ measurement of the fluctuations in the large-scale magnetic field (Horbury et al., 2020); and the radio and plasma waves instrument (RPW) for data on small scale electromagnetic field fluctuations (Maksimovic et al., 2020). These instruments provide datasets of unprecedented temporal and spatial detail giving a novel perspective on solar wind activity (Müller et al., 2020).

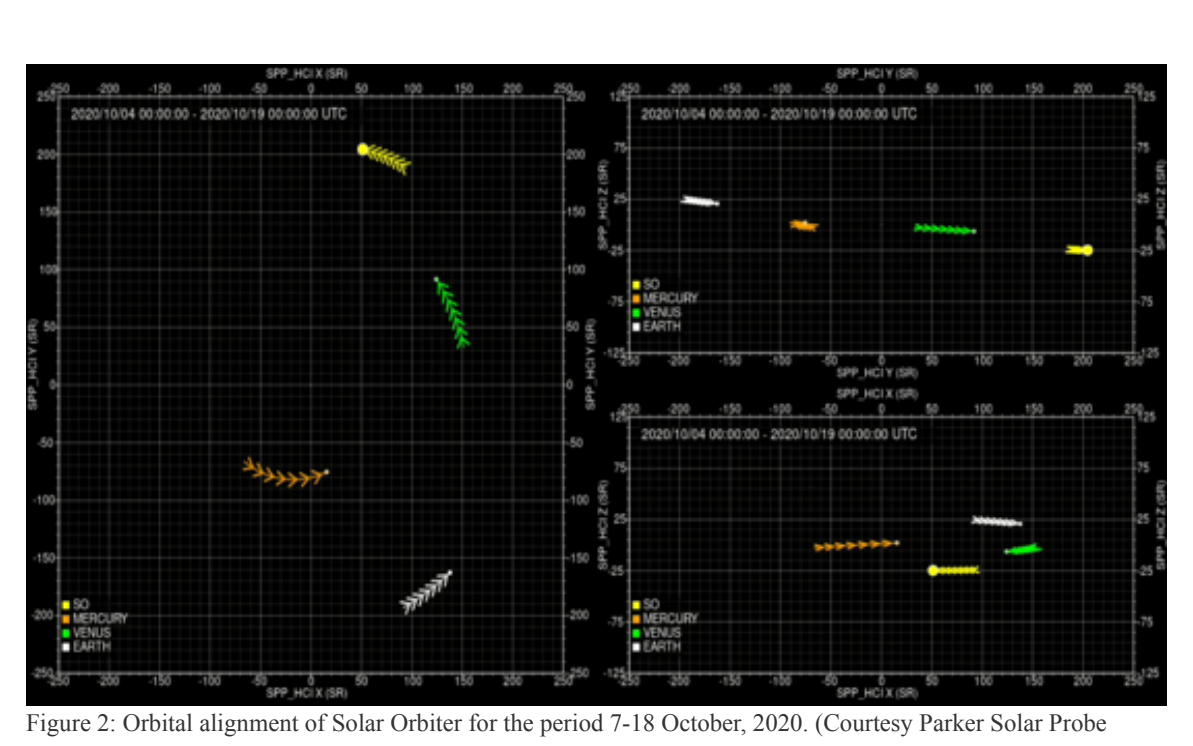

Figure 2: Orbital alignment of Solar Orbiter for the period 7-18 October, 2020. (Courtesy Parker Solar Probe science gateway orbital planning tool)

Owing to early calibration issues all PAS data with SW velocity < 380km/s has been eliminated from analysis and all MAG data used are at quality flag 2 or better. According to the availability of the SWA/PAS ground moments datasets, these criteria have led to a focus on the period 7-18 October 2020 for detailed investigations. The orbital position of the spacecraft at that time is shown as figure 2.

RESULTS 1

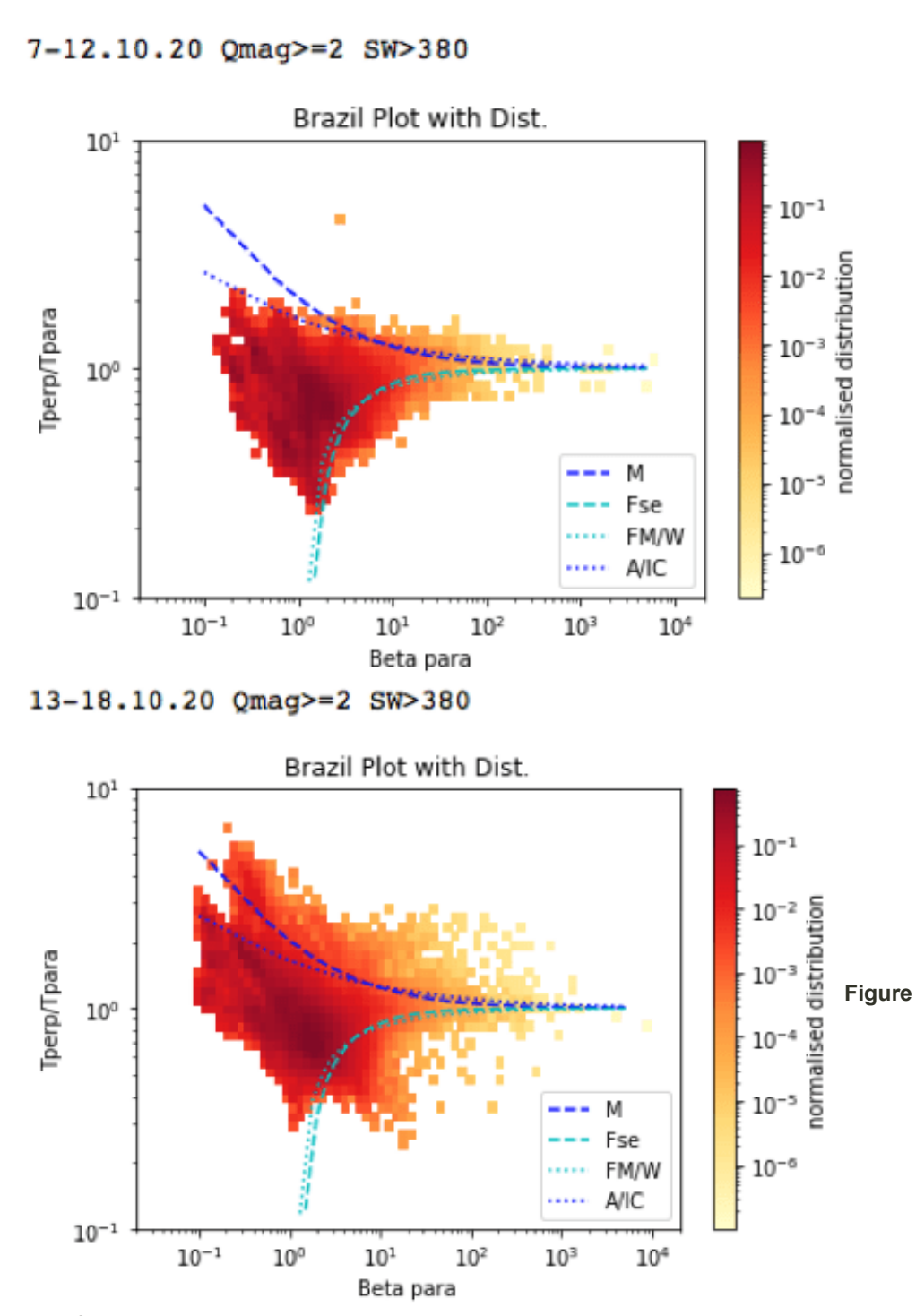

Figure 3: Brazil plots from data analysis as noted

The starting point for this analysis is to create **Anisotropy ($T_\perp/T_{||}$) - Beta ($\beta_{||}$) plots of the relevant data (so-called 'Brazil plots')** and two are shown as figure 3.

For these plots the following parameters are used:

- **$T_\perp/T_{||}$**: Temperature perpendicular to the magnetic field direction divided by temperature parallel to the magnetic field direction with temperatures calculated from the pressure tensor given by the Ground Moments in the SWA/PAS data after rotation to align with magnetic field direction
- **$\beta_{||}$**: $\beta_{||} = 8\pi.K_B.N_p.T_{||} / B^2$

  where κ_B is the Boltzmann constant, N_p is the proton density and B is the magnitude of the magnetic field
- **M** is the mirror mode instability threshold; **A/IC** is the threshold for Alfven/ion-cyclotron waves; **Fse** is the oblique firehose mode instability threshold; **FM/W** is the threshold for fast-magnetosonic/whistler waves
- Instability thresholds are calculated in accordance with Verscharen et al., 2016 for a maximum growth rate of $\Omega_p.10^{-2}$, where Ω_p is the proton gyrofrequency.

The nature of the datapoints which fall in the **'unstable' regions** (i.e. the regions outside the Mirror and Oblique Firehose instability thresholds **where it is expected that wave modes should develop and grow, thereby returning the plasma to the stable regime**) is considered.

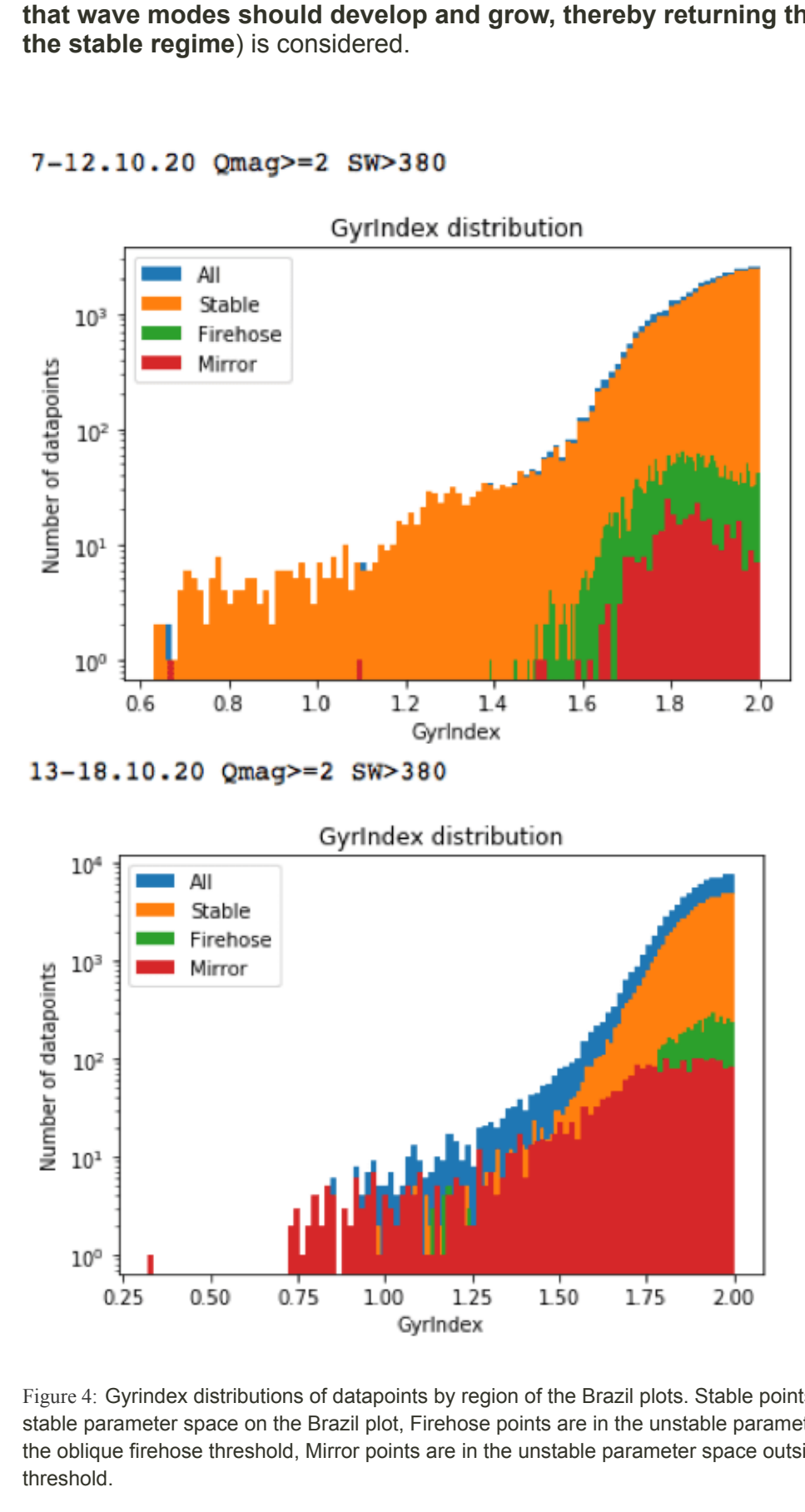

Figure 4: Gyrindex distributions of datapoints by region of the Brazil plots. Stable points are inside the stable parameter space on the Brazil plot, Firehose points are in the unstable parameter space outside the oblique firehose threshold, Mirror points are in the unstable parameter space outside the mirror threshold.

To evaluate the **axisymmetric properties of the plasma** in the direction perpendicular to B_M, the magnitude of the magnetic field, **a measure of gyrotropy, called the Gyrindex (G_{yr}), is developed** using the following equation:

$$G_{yr} = 2 - |(P_{\perp xx} - P_{\perp yy})/0.5(P_{\perp xx} + P_{\perp yy})|$$

Where $P_{\perp xx}$ and $P_{\perp yy}$ are the [1,1] and [2,2] elements of the rotated pressure tensor representing the pressure in the two axes perpendicular to the direction of B_M, and a **maximum gyrindex of 2 is therefore perfectly axisymmetric**.

G_{yr} distributions indicate that those datapoints in the unstable regions are less gyrotropic than the general population of points in the stable region as can be seen in figure 4, where **the peak for distributions of the unstable regions have G_{yr} = ~1.85, whereas the peak for the stable population occurs at G_{yr} = 2**:

The **dependence of the data on the angle between the direction of V_{SW}, the bulk velocity of the solar wind, and the direction of B_M (B/V angle)** is considered. Results are shown below in figure 5:

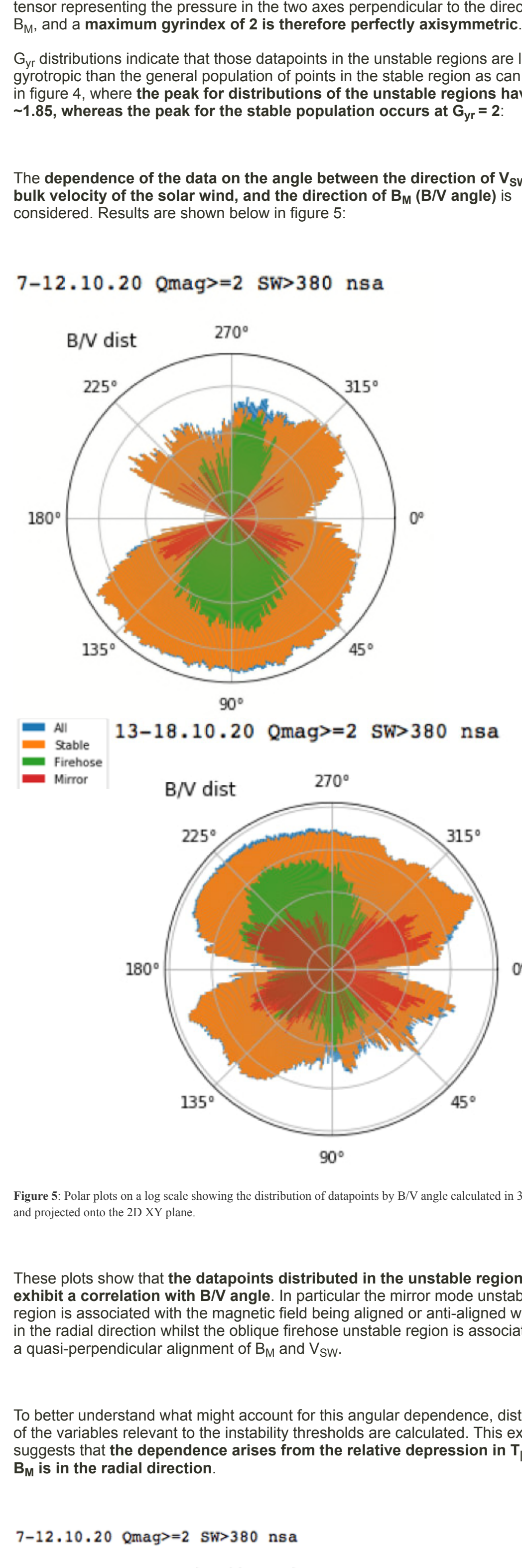

Figure 5: Polar plots on a log scale showing the distribution of datapoints by B/V angle calculated in 3D space and projected onto the 2D XY plane.

These plots show that **the datapoints distributed in the unstable regions exhibit a correlation with B/V angle**. In particular the mirror mode unstable region is associated with the magnetic field being aligned or anti-aligned with V_{SW} in the radial direction whilst the oblique firehose unstable region is associated with a quasi-perpendicular alignment of B_M and V_{SW}.

To better understand what might account for this angular dependence, distributions of the variables relevant to the instability thresholds are calculated. This exercise suggests that **the dependence arises from the relative depression in $T_{||}$ when B_M is in the radial direction**.

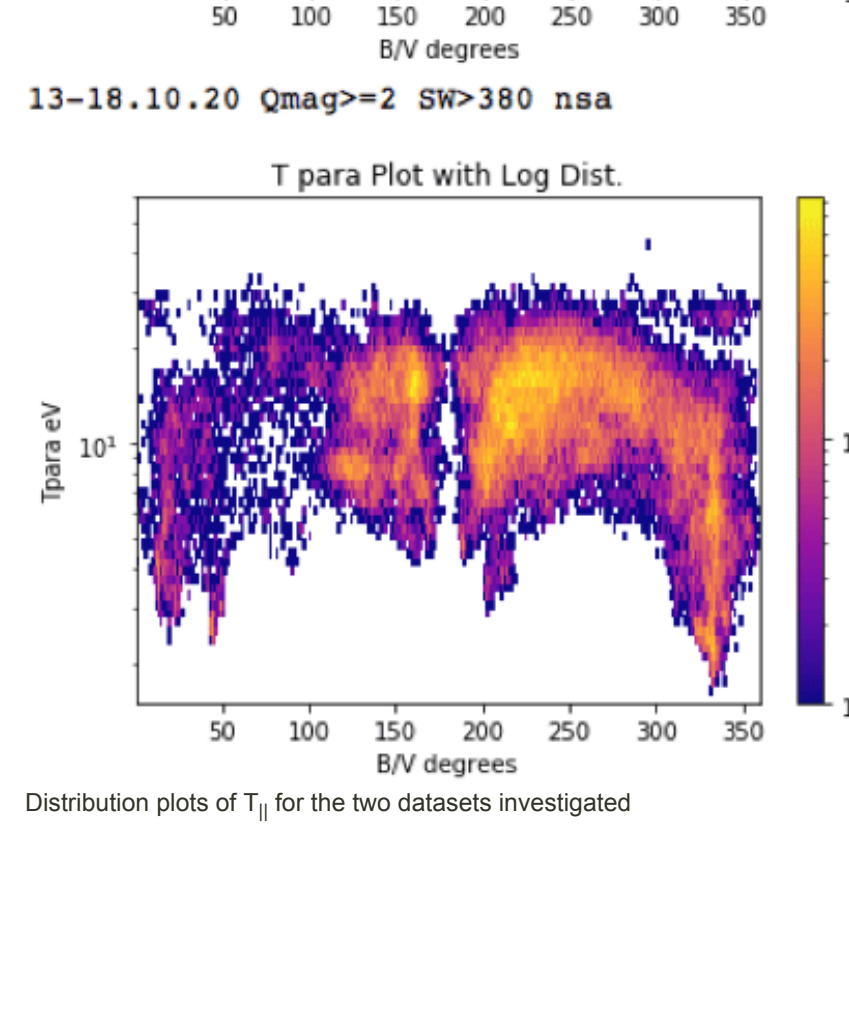

Figure 6: Distribution plots of $T_{||}$ for the two datasets investigated

RESULTS 2

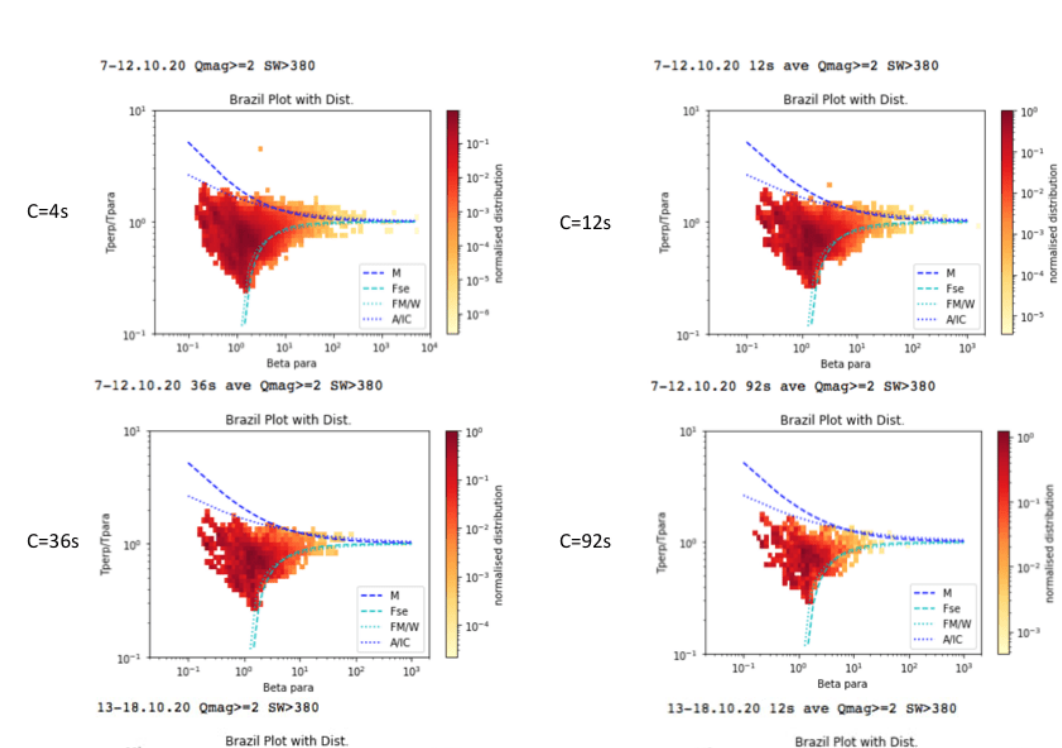

Figure 7: Brazil plots generated from data aggregated over a range of sampling cadences (C) as indicated. Upper 4 panels for 7-12.10.20 and lower 4 panels for 13-18.10.20.

Subsequent investigation has focussed on **whether the datapoints found in the unstable regions are transient features registered by the PAS instrument's 4 second cadence not previously been seen in lower resolution data such as that from the WIND spacecraft** which has a 92 second sampling cadence. Aggregated datasets are formed as follows:

- New input datasets are formed from the cdf files containing the base variables (VAR_{base})
- The base high resolution files are at a 4 second cadence as determined by the SWA PAS instrument
- New variables (VAR_{new}) are calculated by summing and averaging the base variables to required cadences

Brazil plots of the data at a range of selected cadences are produced as shown in figure 7. These plots suggest that as temperature anisotropies develop in a plasma parcel **some of the particles that move into the 'unstable' parameter space outside the instability thresholds may not remain there for sufficient time to allow instability wave modes to develop**. These particles occupy the 'unstable' space without in fact becoming technically unstable, where technically unstable is defined by exhibiting the applicable instability wave modes.

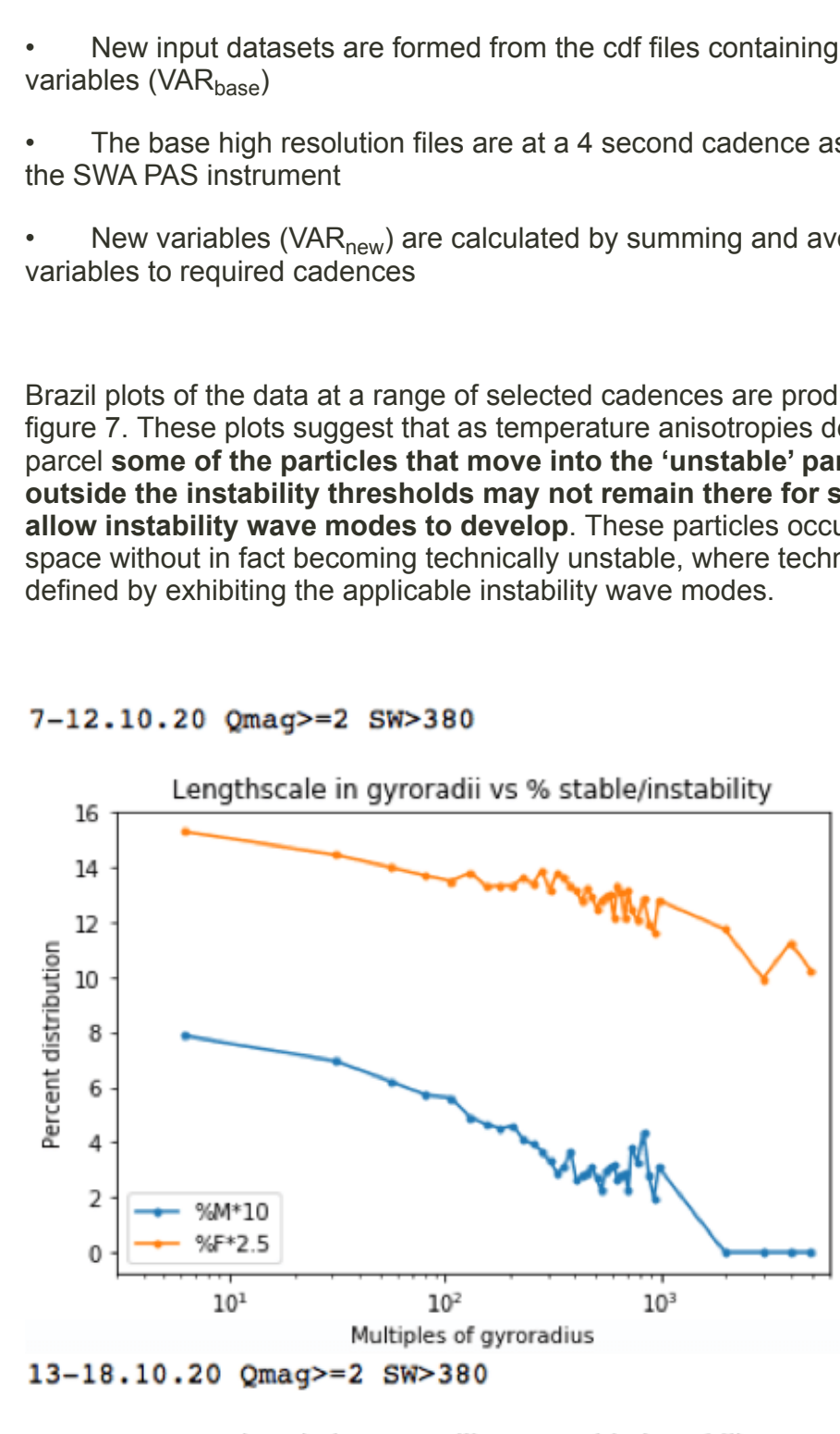

Figure 8: The proportion of datapoints in the Mirror (M) and Oblique Firehose (F) regions expressed as a percentage, scaled for clarity, plotted as a function of lengthscale of the measurement frame in proton gyroradii.

The **residence time in 'unstable' regions is also a measure of the available space for wave instabilities to develop** – or the size of the box for a given parcel of plasma. A comprehensive range of scales is developed with timescales converted pointwise into lengthscales measured in proton gyroradii. The result of this analysis is given in figure 8.

The two plots show that the rate of decrease of the number of unstable region datapoints as a proportion of the total sample, increases with lengthscale. Further, **there is an apparent breakpoint at ~10^2 gyroradii at which the rate of decrease increases exponentially**.

The wavelength (λ_W) of waves at the maximum growth rate of instability in terms of proton gyroradii (G_{pr}), to a reasonable approximation is given by:

$$\lambda_w \cong (2\pi/0.5).G_{pr}$$

(Gary, 1993; Pokhotelov, 2004; Stacey, 2012)

which gives:

$$10^2.\ G_{pr} \cong 8.\ \lambda_w$$

Suggesting that **the lengthscale of the space required for instability wave modes to grow may be around 8 wavelengths**

DISCUSSION

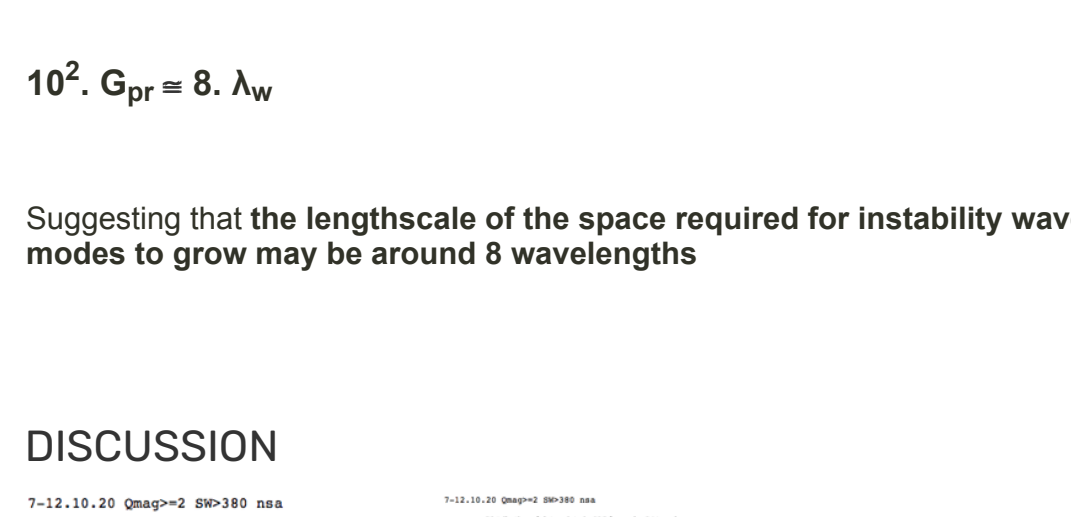

Figure 9: Structure of B/V angle dependence in Brazil plot dataspace shown for both datasets.

Further work is needed to identify and evaluate the potential causes of the observed agyrotropy; as well as the depression of $T_{||}$ when B_M is aligned in the radial direction, which is primarily responsible for the observed dependence on the B/V angle of datapoints in the unstable regions. The structure of the dependence in parameter space is shown in figure 9.

CONCLUSION

- The Mirror and Oblique Firehose 'unstable' regions are characterised by conditions that indicate the presence of unstable modes - temperature anisotropy, agyrotropy - but 'technical instability' exhibits latency related to the lengthscale required for wave instabilities to develop.
- This lengthscale requirement may help constrain relevant scales for the assumption of homogeneity in the turbulent solar wind, which is needed for instabilities to grow.
- At the spatial and temporal resolution of Solar Orbiter SWA/PAS data, processes that relate to wave/particle interactions can reveal significant information about the sub-ion scales in the solar wind.
- This information can improve the current understanding of what conditions are needed for instabilities to act.

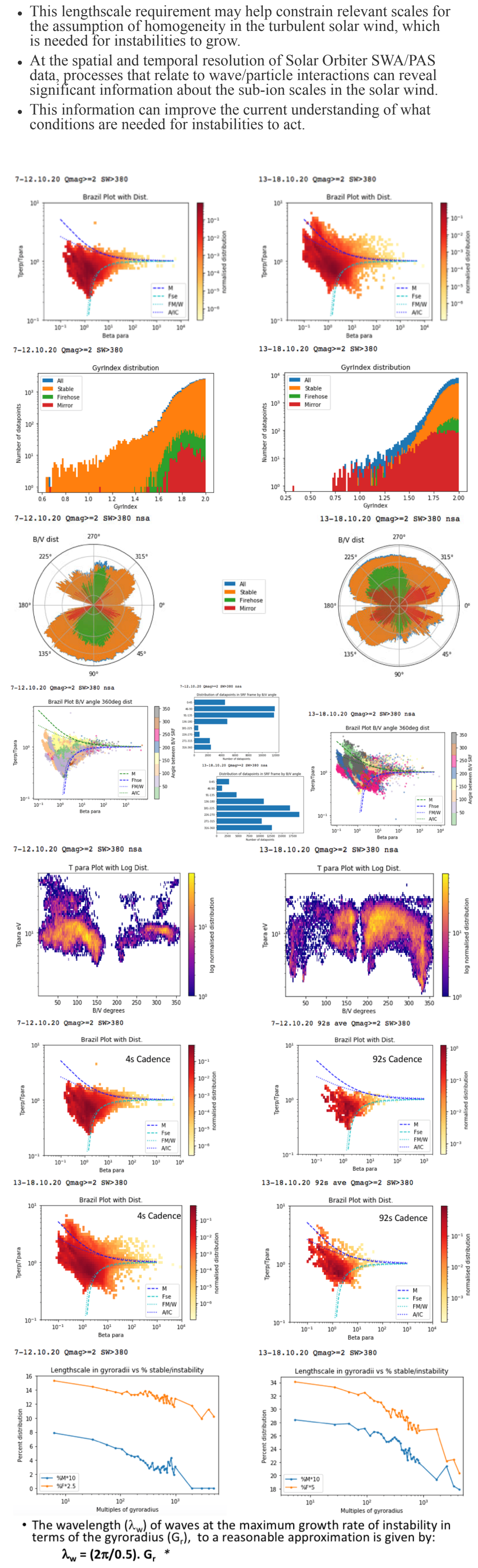

- The wavelength (λ_w) of waves at the maximum growth rate of instability in terms of the gyroradius (G_r), to a reasonable approximation is given by:

  $\lambda_w = (2\pi/0.5).\ G_r$ *

- There is a breakpoint at ~10^2 gyroradii at which the rate of relative decline of unstable points increases sharply. This gives:

  $10^2.\ G_r \cong 8.\ \lambda_w$

- Suggesting that the lengthscale of the space required for instability wave modes to grow may be around 8 wavelengths.

* Gary, 1993 ; Pokhotelov et al., 2004; Stacey, 2005

AUTHOR INFORMATION

Simon Opie, Department of Space and Climate Physics, Mullard Space Science Laboratory, University College London, Dorking RH5 6NT, UK;

Daniel Verscharen, Department of Space and Climate Physics, Mullard Space Science Laboratory, University College London, Dorking RH5 6NT, UK;

Chris Chen, Department of Physics and Astronomy, Queen Mary University of London, London E1 4NS, UK;

Christopher Owen, Department of Space and Climate Physics, Mullard Space Science Laboratory, University College London, Dorking RH5 6NT, UK.

ABSTRACT

The solar wind is a continuous outflow of plasma from the Sun, which expands into the space between the planets in our solar system and forms the heliosphere. The solar wind is inherently turbulent and characterised by kinetic micro-instabilities on a range of scales. The Sun also intermittently ejects mass (coronal mass ejections; CMEs) or solar energetic particles (SEPs) which change their trajectory or energy due to their interactions with the solar wind. When these violent particle events hit the Earth's magnetosphere, they can cause "space weather" with both long- and short-term impacts on our natural and technological environment. This presentation investigates the behaviour and the effects of kinetic instabilities in a turbulent plasma with particular emphasis on energy transfer processes. We utilise the unprecedented observations from ESA's Solar Orbiter spacecraft, launched in February 2020, to advance our understanding of the Sun, the solar wind, and space weather.

Large-scale compressions (ubiquitous in solar-wind turbulence) create conditions for proton, alpha-particle and electron microinstabilities, which then transfer energy to small-scale fluctuations. These instability-driven small-scale fluctuations, including those driven by turbulence and other sources of free energy (e.g. particle beams, differential flows, heat fluxes, temperature anisotropies), make a significant contribution to the fluctuation spectrum at kinetic scales, where energy dissipation occurs.

We consider instabilities driven by turbulence in the plasma by using statistical methods to analyse the Solar Orbiter data and characterise the turbulence at the relevant scales and amplitude. Specifically, we evaluate the processes by which turbulence combined with temperature anisotropy causes instability, comparing theoretical calculations with the high resolution data available from the Solar Orbiter MAG and SWA instruments.

REFERENCES

Gary, S.P., 1993. Theory of space plasma microinstabilities, Cambridge atmospheric and space science series. Cambridge University Press, Cambridge [England]; New York.

Horbury, T.S., O'Brien, H., Carrasco Blazquez, I., Bendyk, M., Brown, P., Hudson, R., Evans, V., Oddy, T.M., Carr, C.M., Beek, T.J., Cupido, E., Bhattacharya, S., Dominguez, J.-A., Matthews, L., Myklebust, V.R., Whiteside, B., Bale, S.D., Baumjohann, W., Burgess, D., Carbone, V., Cargill, P., Eastwood, J., Erdös, G., Fletcher, L., Forsyth, R., Giacalone, J., Glassmeier, K.-H., Goldstein, M.L., Hoeksema, T., Lockwood, M., Magnes, W., Maksimovic, M., Marsch, E., Matthaeus, W.H., Murphy, N., Nakariakov, V.M., Owen, C.J., Owens, M., Rodriguez-Pacheco, J., Richter, I., Riley, P., Russell, C.T., Schwartz, S., Vainio, R., Velli, M., Vennerstrom, S., Walsh, R., Wimmer-Schweingruber, R.F., Zank, G., Müller, D., Zouganelis, I., Walsh, A.P., 2020. The Solar Orbiter magnetometer. Astronomy & Astrophysics 642, A9. https://doi.org/10.1051/0004-6361/201937257

Maksimovic, M., Bale, S., Chust, T., Khotyaintsev, Y., Krasnoselskikh, V., Kretzschmar, M., Plettemeier, D., Rucker, H., Souček, J., Steller, M., others, 2020. The Solar Orbiter Radio and Plasma Waves (RPW) instrument. Astronomy & Astrophysics 642, A12.

Müller, D., St. Cyr, O.C., Zouganelis, I., Gilbert, H.R., Marsden, R., Nieves-Chinchilla, T., Antonucci, E., Auchère, F., Berghmans, D., Horbury, T.S., Howard, R.A., Krucker, S., Maksimovic, M., Owen, C.J., Rochus, P., Rodriguez-Pacheco, J., Romoli, M., Solanki, S.K., Bruno, R., Carlsson, M., Fludra, A., Harra, L., Hassler, D.M., Livi, S., Louarn, P., Peter, H., Schühle, U., Teriaca, L., del Toro Iniesta, J.C., Wimmer-Schweingruber, R.F., Marsch, E., Velli, M., De Groof, A., Walsh, A., Williams, D., 2020. The Solar Orbiter mission: Science overview. Astronomy & Astrophysics 642, A1. https://doi.org/10.1051/0004-6361/202038467

Owen, C.J., Bruno, R., Livi, S., Louarn, P., Al Janabi, K., Allegrini, F., Amoros, C., Baruah, R., Barthe, A., Berthomier, M., Bordon, S., Brockley-Blatt, C., Brysbaert, C., Capuano, G., Collier, M., DeMarco, R., Fedorov, A., Ford, J., Fortunato, V., Fratter, I., Galvin, A.B., Hancock, B., Heirtzler, D., Kataria, D., Kistler, L., Lepri, S.T., Lewis, G., Loeffler, C., Marty, W., Mathon, R., Mayall, A., Mele, G., Ogasawara, K., Orlandi, M., Pacros, A., Penou, E., Persyn, S., Petiot, M., Phillips, M., Přech, L., Raines, J.M., Reden, M., Rouillard, A.P., Rousseau, A., Rubiella, J., Seran, H., Spencer, A., Thomas, J.W., Trevino, J., Verscharen, D., Wurz, P., Alapide, A., Amoruso, L., André, N., Anekallu, C., Arciuli, V., Arnett, K.L., Ascolese, R., Bancroft, C., Bland, P., Brysch, M., Calvanese, R., Castronuovo, M., Čermák, I., Chornay, D., Clemens, S., Coker, J., Collinson, G., D'Amicis, R., Dandouras, I., Darnley, R., Davies, D., Davison, G., De Los Santos, A., Devoto, P., Dirks, G., Edlund, E., Fazakerley, A., Ferris, M., Frost, C., Fruit, G., Garat, C., Génot, V., Gibson, W., Gilbert, J.A., de Giosa, V., Gradone, S., Hailey, M., Horbury, T.S., Hunt, T., Jacquey, C., Johnson, M., Lavraud, B., Lawrenson, A., Leblanc, F., Lockhart, W., Maksimovic, M., Malpus, A., Marcucci, F., Mazelle, C., Monti, F., Myers, S., Nguyen, T., Rodriguez-Pacheco, J., Phillips, I., Popecki, M., Rees, K., Rogacki, S.A., Ruane, K., Rust, D., Salatti, M., Sauvaud, J.A., Stakhiv, M.O., Stange, J., Stubbs, T., Taylor, T., Techer, J.-D., Terrier, G., Thibodeaux, R., Urdiales, C., Varsani, A., Walsh, A.P., Watson, G., Wheeler, P., Willis, G., Wimmer-Schweingruber, R.F., Winter, B., Yardley, J., Zouganelis, I., 2020. The Solar Orbiter Solar Wind Analyser (SWA) suite. Astronomy & Astrophysics 642, A16. https://doi.org/10.1051/0004-6361/201937259

Pokhotelov, O.A., 2004. Mirror instability at finite ion-Larmor radius wavelengths. J. Geophys. Res. 109, A09213. https://doi.org/10.1029/2004JA010568

Stacey, W.M., 2012. Fusion plasma physics. Wiley-VCH, Weinheim, Germany.

Verscharen, D., Chandran, B.D.G., Klein, K.G., Quataert, E., 2016. COLLISIONLESS ISOTROPIZATION OF THE SOLAR-WIND PROTONS BY COMPRESSIVE FLUCTUATIONS AND PLASMA INSTABILITIES. The Astrophysical Journal 831, 128. https://doi.org/10.3847/0004-637X/831/2/128

LINK TO A SURVEY

Enter your survey URL here

https://example.com

Submit

Delete